Modelling and control of a tethered drone for an AWE application

Zakeye Azaki, Jonathan Dumon, Nacim Meslem, Ahmad Hably, Pierre Susbielle

Modelling and control of a tethered drone for an AWE application

Zakeye AZAKI, Jonathan DUMON, Nacim MESLEM, Ahmad HABLY, Pierre SUSBIELLE
Univ. Grenoble Alpes, CNRS, Grenoble-INP
GIPSA-lab, F-38000, Grenoble, France
(zakeye.azaki,jonathan.dumon,nacim.meslem,ahmad.hably,pierre.susbielle)@gipsa-lab.grenoble-inp.fr

***Abstract*—This paper proposes a nonlinear control strategy to achieve autonomous take-off and landing of a drone-based tethered Magnus flying device. This flying device is used in airborne wind energy system that converts wind energy into electricity. A 3D model is constructed and used to design a feedback linearization controller to obtain the desired flight trajectories. Simulation results with an illustrated realistic model indicate good performance and robustness in different flying conditions. This complex and realistic simulation environment supports real experimental testing.**

***Index Terms*—Airborne Wind Energy system (AWE), nonlinear system, nonlinear control, system modeling, Modeling identification, actuator compensation**

I. Introduction

The goal of extensive research and development efforts nowadays is directed into producing huge amounts of cost-competitive electrical power. Airborne Wind Energy (AWE) systems convert wind energy at high altitude into electrical energy using autonomous tethered aircraft [3], [12]. These systems provide a viable approach for reducing the amount of material requirements per unit of power. Because tethered devices' flying operations may be changed due to different wind conditions, one of the key research and development goals right now, in AWE society, is the total autonomous and reliable functioning. This represents a rich topic in automatic control strategies that must function robustly in all power generation phases and under extreme operating conditions. Most of the literature surrounding the field of AWE system, has introduced control strategies that enable AWE systems to fly in prescribed paths for power generation phase [14], [13]. Fewer researches assign the take-off and landing phases of the AWE systems [4], [7], [11].

The main contribution of this paper, compared to other studies illustrated in literature, is highlighted in proposing a 3D nonlinear controller of drone-based rigid wing AWE system with on-ground generation system in the take-off and landing phases. This system can take-off and land under specific wind field characteristics and even without wind. The on-ground winch is used to control the tether's reel-in and reel-out lengths. Hence, the system's model is composed of the flying device and the coupled ground winch. The flying device is different from those studied in the literature due to the existence of a Magnus fixed to the drone.

Paper Organization: This paper is organized as follows. In Section II, we illustrate the overall system's complex model. The design of robust feedback linearization (FL) controller based on simplified system's model is discussed in section III. Finally, section IV presents a series of realistic simulations to illustrate the performance and to validate the robustness of the control strategy against specific wind fields. The paper ends with some conclusions.

II. System Modeling

The drone-based AWE system studied in this paper is composed of two elements: The first element is a flying device composed of a drone of mass m_D fixed to any rigid wing. In this paper we consider a Magnus of mass m_M as the fixed wing. The second one is an on-ground station of inertia I_G and center of gravity C_G. Both elements are connected through a tether as shown in Fig. 1. The tether is attached to the flying device at the drone's center of gravity C_B.

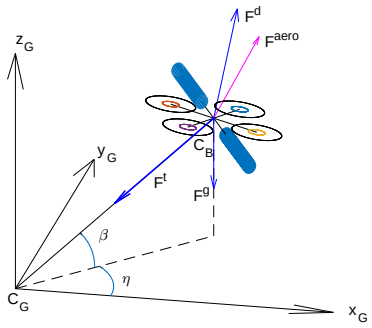

Fig. 1: Free body diagram of drone based Magnus AWE system

A. Reference Frames

We include three right-handed reference frames for more clarity in presenting the model and control strategy:

- **Global Frame** $\mathcal{G}(\vec{x}_\mathcal{G}, \vec{y}_\mathcal{G}, \vec{z}_\mathcal{G})$ **-** It is an inertial Cartesian coordinate system, where $\vec{x}_\mathcal{G}$ is aligned with the wind velocity. Its origin coincides with the on-ground station C_G.
- **Local or tether Frame** $\mathcal{L}(\vec{x}_\mathcal{L}, \vec{y}_\mathcal{L}, \vec{z}_\mathcal{L})$ **-** It is the non-inertial coordinate system fixed to the drone. where $\vec{x}_\mathcal{L}$ is aligned with tether and pointing away from the on-ground station.
- **Body Frame** $\mathcal{B}(\vec{x}_\mathcal{B}, \vec{y}_\mathcal{B}, \vec{z}_\mathcal{B})$ **-** It is non-inertial coordinate system centered at C_B. Where $\vec{x}_\mathcal{B}$ points towards C_G and corresponds to the longitudinal axis of the aircraft, $\vec{y}_\mathcal{B}$ is an orthogonal axis to the first one and aligned with the Magnus axis of rotation and $\vec{z}_\mathcal{B}$ axis is aligned with the propeller's axis .

The relative orientation between frames $\mathcal{G}$ and $\mathcal{B}$ can be expressed by the Euler angles ϕ, θ and ψ. These angles represent the

rotational position of the drone in $\mathcal{G}$ frame. Thus any vector $\vec{F}_{\mathcal{G}}$ in $\mathcal{G}$ system can be translated into vector $\vec{F}_{\mathcal{B}}$ in $\mathcal{B}$ system through the following ZYX rotation matrix:

$$R_{\mathcal{GB}} = \begin{bmatrix} c_\theta c_\psi & c_\theta s_\psi & -s_\theta \\ s_\phi s_\theta c_\psi - c_\phi s_\psi & s_\phi s_\theta s_\psi + c_\phi c_\psi & s_\phi c_\theta \\ c_\phi s_\theta c_\psi + s_\phi s_\psi & c_\phi s_\theta s_\psi - s_\phi c_\psi & c_\phi c_\theta \end{bmatrix} \quad (1)$$

where 's' and 'c' refer respectively to sine and cosine functions. Therefore, $\vec{F}_{\mathcal{B}}$= $R_{\mathcal{GB}} * \vec{F}_{\mathcal{G}}$, where $*$ denotes the matrix multiplication. Moreover, the rotation matrix from $\mathcal{G}$ to $\mathcal{L}$ is given as follows:

$$R_{\mathcal{GL}} = \begin{bmatrix} c_\eta c_\beta & s_\eta c_\beta & s_\beta \\ -s_\eta & c_\eta & 0 \\ -c_\eta s_\beta & -s_\eta s_\beta & c_\beta \end{bmatrix} \quad (2)$$

B. Tether Model

The tether of length r is assumed to be taut and approximated as straight line. Although tether's sag can have a significant impact on the flight dynamic states of the aircraft, this assumption could still be of less importance for small tether's length where the linear mass is negligible.

C. Drone Model

The following considerations about modelling are mainly taken from [8] and [9].

1) Actuator to body dynamics: a quad-rotor drone is a flying platform actuated by four motors and propellers. Let $\mathbf{w}_D = [w_1 \quad w_2 \quad w_3 \quad w_4]^T$ be respectively the rotation speed of each actuator. A simple lift and drag propeller model as expressed and used for UAV modelling in [9] and [5] allows us to estimate for each actuator $i = 1, 2, 3, 4$, a force $\vec{F}_i$ and a torque $\vec{\Gamma}_i$:

$$\begin{aligned} \vec{F}_i &= c_T w_i^2 \vec{z}_{\mathcal{B}} \\ \vec{\Gamma}_i &= c_Q w_i^2 \vec{z}_{\mathcal{B}} \end{aligned} \quad (3)$$

where c_T and c_Q are the propeller thrust and drag coefficient respectively. The actuators' forces and torques can be linearly combined to obtain a total thrust force $\vec{F}^d_{\mathcal{B}} = T_D^{sys} \vec{z}_{\mathcal{B}}$, and three rotational torques $\vec{\Gamma}_c = [\Gamma_p \quad \Gamma_q \quad \Gamma_r]^T$, where T_D^{sys} is the actual total thrust force generated by the four drone's propellers

$$\begin{bmatrix} T_D^{sys} \\ \Gamma_p \\ \Gamma_q \\ \Gamma_r \end{bmatrix} \simeq \underbrace{\begin{bmatrix} c_T & c_T & c_T & c_T \\ -c_T l_D & c_T l_D & c_T l_D & -c_T l_D \\ -c_T l_D & -c_T l_D & c_T l_D & c_T l_D \\ c_Q & -c_Q & c_Q & -c_Q \end{bmatrix}}_{M_x} \begin{bmatrix} \omega_1^2 \\ \omega_2^2 \\ \omega_3^2 \\ \omega_4^2 \end{bmatrix} \quad (4)$$

where l_D is the lever arm size between an actuator and the drone center of mass C_B. Those forces and torques are control variables for the drone angular velocities model. The behaviour of the actuator rotation speed is represented with the one phase equivalent model of a brushless actuators, as used in [2].

2) Angular velocities loop in $\mathcal{B}$: In the body frame $\mathcal{B}$, let us define $\vec{\Omega} = [p \quad q \quad r]^T$, the representation of angular velocities respectively about $\vec{x_{\mathcal{B}}}$, $\vec{y_{\mathcal{B}}}$ and $\vec{z_{\mathcal{B}}}$. Angular velocities dynamics is expressed as

$$\dot{\vec{\Omega}} = -J^{-1} \Omega^{\times} J \vec{\Omega} + J^{-1} \vec{\Gamma}_c \quad (5)$$

Where J represents the inertia matrix of the drone body and $\Omega^{\times}$ the skew symmetric matrix made of $\vec{\Omega}$. Therefore, angular velocities in $\mathcal{B}$ can be controlled with $\vec{\Gamma}_c$

3) Angular position loop in $\mathcal{G}$: From angular velocities $\vec{\Omega}$ in $\mathcal{B}$, one might express the equation of angular position in $\mathcal{G}$. Based on the Euler ZYX formalism,

$$\begin{cases} \begin{bmatrix} \dot{\phi} \\ \dot{\theta} \\ \dot{\psi} \end{bmatrix} &= W^{-1} \vec{\Omega} \\ W^{-1}(\phi, \theta, \psi) &= \begin{bmatrix} 1 & s_\phi t_\theta & c_\phi t_\theta \\ 0 & c_\phi & -s_\phi \\ 0 & s_\phi / c_\theta & c_\phi / c_\theta \end{bmatrix} \end{cases} \quad (6)$$

with $t\theta = tan(\theta)$ and $W(\phi, \theta, \psi)$ known as the Wronskien matrix of the Euler angle attitude representation. Therefore, angular positions in $\mathcal{G}$ can be controlled with $\vec{\Omega}$.

D. Magnus Model

In this work we only consider one Magnus wing attached to the drone of length l_M and base radius r_M. Detailed study of the physical behavior of the Magnus is not considered in this work. However, we recapitulate the model of its drag and lift illustrated in [6]. The aerodynamic forces $\vec{F}^{aero}$ that acts on the flying device is a function of the angular velocity w_M of the Magnus

$$\vec{F}^{aero}_{\mathcal{B}}(w_M) = \vec{F}_L(w_M) + \vec{F}_D(w_M) + \vec{F}_{dy}(w_M) \quad (7)$$

where $\vec{F}_L$ and $\vec{F}_D$ present the lift and drag forces respectively. These forces are expressed in $(\vec{x}_{\mathcal{B}}, \vec{z}_{\mathcal{B}})$ plane. $\vec{F}_{dy}$ is the drag force acting on the drone in $\vec{y}_{\mathcal{B}}$ direction. In $\mathcal{L}$ frame, $\vec{F}^{aero}$ reads

$$\vec{F}^{aero}_{\mathcal{L}}(w_M) = \begin{bmatrix} d_r & d_\eta & d_\beta \end{bmatrix}^T \quad (8)$$

E. On-ground Station Model

The motor-winch subsystem model is approximated according to the following equation

$$\dot{u}_r^{sys} = \frac{1}{\tau_{u_r}} (u_r - u_r^{sys}) \quad (9)$$

where u_r is the control reference torque of the ground winch divided by its radius r_G and u_r^{sys} is the actual effected torque. Hence, the actual tether traction force is derived from the rotational equilibrium as follows

$$T_{th} = u_r^{sys} + m_G \ddot{r} + \Gamma_s \quad (10)$$

such that $m_G = \frac{I_G}{r_G^2}$ and Γ_s represents the dry friction of the ground winch.

III. Control Strategy

In this section we will illustrate the overall implemented control strategy illustrated in Fig. 2.

A. Inner Control Loops of the Drone

Most of the drones are controlled via a hierarchical control strategy divided into slow (outer loop) and fast (inner loop) dynamics. In our work, to fit with classical experimental setup, the two inner loops (secs. II-C2 and II-C3) are considered closed and well controlled. For simulation purposes, we implant the ROS/PX4 architecture as used in GIPSA-Lab experimental aerial robotics platform [10]. The inner control architecture is taken from [1]. In the control design, the inner dynamics is considered as three actuator forces in the tether frame. This approximation is described later in (20).

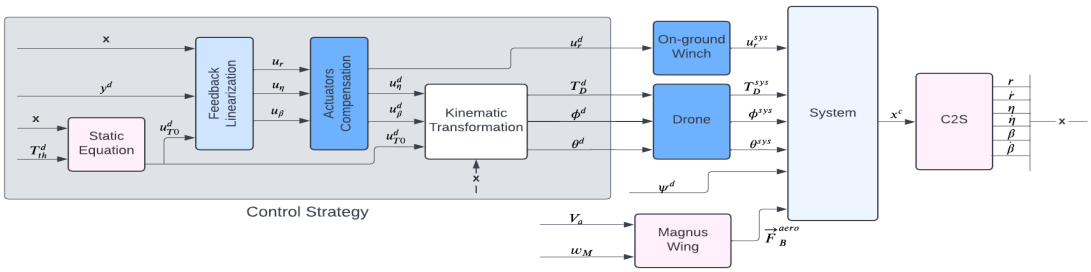

Fig. 2: Block diagram describing the control strategy

B. System Setup

The system's state is determined by three degrees of freedom: the position describing the drone point mass C_B

$$\vec{\mathbf{p}}_{\mathcal{G}} = \begin{bmatrix} x \\ y \\ z \end{bmatrix} = \begin{bmatrix} r c_\beta c_\eta \\ r c_\beta s_\eta \\ r s_\beta \end{bmatrix} \tag{11}$$

This position is parameterized by the spherical coordinates r, η and β where η and β are respectively the relative elevation and azimuth angles of the tether. For the control strategy, that will be presented in the following subsections, it is useful to convert the Cartesian coordinates in frame $\mathcal{G}$ to spherical coordinates:

$$\begin{bmatrix} r \\ \eta \\ \beta \end{bmatrix} = \begin{bmatrix} \sqrt{x^2+y^2+z^2} \\ \arctan 2(y,x) \\ \arctan\left(\frac{z}{\sqrt{x^2+y^2}}\right) \end{bmatrix} \tag{12}$$

where $\arctan 2(.,.)$ is the four-quadrant arctangent function. Thus, the local acceleration of the flying device, derived from the double derivative of (11), reads as

$$\ddot{\vec{\mathbf{p}}}_{\mathcal{L}} = \begin{bmatrix} \ddot{r} \\ r\ddot{\eta} c_\beta \\ r\ddot{\beta} \end{bmatrix} + \underbrace{\begin{bmatrix} -r\dot{\beta}^2 - r\dot{\eta}^2 c_\beta^2 \\ 2\dot{r}\dot{\eta}c_\beta - 2r\dot{\eta}\dot{\beta}s_\beta \\ 2\dot{r}\dot{\beta} + r\dot{\eta}^2 c_\beta s_\beta \end{bmatrix}}_{-\frac{1}{m}\vec{F}_{\mathcal{L}}^{inert}} \tag{13}$$

where the second part corresponds to the Coriolis and centrifugal forces stated as inertial forces $\vec{F}^{inert}$.

C. Model used to Design the Controller

In this section we will present a simplified model which has been specifically derived for the control design task of take-off and landing phases of the AWE system. This control strategy will be fully illustrated in the following subsections. For the sake of the control design, all the external disturbances, i.e., aerodynamic and friction forces, are neglected. Moreover, the dynamic of u_r^{sys} is also neglected, so $u_r^{sys} = u_r$. Thus, For this section we define the total force acting on the drone in any reference frame, as shown in Fig. 1, as,

$$m_B \ddot{\vec{\mathbf{p}}} = \vec{F}^g + \vec{F}^t + \vec{F}^d \tag{14}$$

The gravitational Force $\vec{F}^g$ and the tether force $\vec{F}^t$ can be described as,

$$\begin{aligned} \vec{F}_{\mathcal{G}}^g &= -m_B g \vec{z}_{\mathcal{G}} \\ \vec{F}_{\mathcal{L}}^t &= -T_{th} \vec{x}_{\mathcal{L}} \end{aligned} \tag{15}$$

where $m_B = m_D + m_M$ is the mass of the overall flying device, g is the gravity acceleration and T_{th} represents the tension force at the ground station presented in (10). The total thrust force due to the four drone's propellers $\vec{F}_{\mathcal{B}}^d = T_D \vec{z}_{\mathcal{B}}$ where T_D is the control reference thrust force, assuming that the drone's dynamics are neglected, i.e, $T_D^{sys} = T_D$. Then we can use the transformations in (1) and (2) to determine $\vec{F}_{\mathcal{L}}^d = R_{\mathcal{GL}} * R_{\mathcal{BG}} * \vec{F}_{\mathcal{B}}^d$. We represent the total thrust force in $\mathcal{L}$ frame as,

$$\vec{F}_{\mathcal{L}}^d = [u_{T0} \quad u_\eta \quad u_\beta]^T \tag{16}$$

Considering all the external forces described in (10), (15) and (16). Equation (13) allows us to redefine Newton's second law of motion in (14) in the $\mathcal{L}$ frame as

$$m_B \begin{bmatrix} \ddot{r} \\ r\ddot{\eta}c_\beta \\ r\ddot{\beta} \end{bmatrix} = \vec{F}_{\mathcal{L}}^{inert} + \vec{F}_{\mathcal{L}}^g + \vec{F}_{\mathcal{L}}^t + \vec{F}_{\mathcal{L}}^d \tag{17}$$

D. Control Design

Considering the state vector as $\mathbf{x} = [r \quad \dot{r} \quad \eta \quad \dot{\eta} \quad \beta \quad \dot{\beta}]^T$, the considered output as $\mathbf{y} = [r \quad \eta \quad \beta]^T$ and the Aerodynamic forces $\vec{F}^{aero}$ and the friction as external disturbances. Equation (17) is easily expressed into the state space representation in $\mathcal{L}$ frame as follows,

$$\begin{bmatrix} \ddot{r} \\ \ddot{\eta} \\ \ddot{\beta} \end{bmatrix} = \underbrace{\begin{bmatrix} \frac{1}{m_B+m_W}[m_B(r\dot{\beta}^2 + r\dot{\eta}^2 c_\beta^2) - m_B g s\beta + u_{T0}] \\ \frac{1}{rc_\beta}[-2\dot{r}\dot{\eta}c_\beta + 2r\dot{\eta}\dot{\beta}s_\beta] \\ -\frac{1}{r}[2\dot{r}\dot{\beta} + r\dot{\eta}^2 c_\beta s_\beta + g c_\beta] \end{bmatrix}}_{b(\mathbf{x})} + \underbrace{\begin{bmatrix} -\frac{1}{m_B+m_W} & 0 & 0 \\ 0 & \frac{1}{m_B r c\beta} & 0 \\ 0 & 0 & \frac{1}{m_B r} \end{bmatrix}}_{A(\mathbf{x})} \left(\underbrace{\begin{bmatrix} u_r \\ u_\eta \\ u_\beta \end{bmatrix}}_{\mathbf{u}} + \underbrace{\begin{bmatrix} -d_r \\ d_\eta \\ d_\beta \end{bmatrix}}_{\mathbf{d}} \right) \tag{18}$$

$$\mathbf{y} = \begin{bmatrix} 1 & 0 & 0 & 0 & 0 & 0 \\ 0 & 0 & 1 & 0 & 0 & 0 \\ 0 & 0 & 0 & 0 & 1 & 0 \end{bmatrix} \mathbf{x} \tag{19}$$

Because of the fact that actuators dynamics were neglected in the model used for control design, lets start by introducing the actuators compensation block. We used model identification technique to approximate the dynamics of η-loop and β-loop as first order models,

$$\dot{u}_\eta^{sys} = \frac{1}{\tau_{u_\eta}}[u_\eta - u_\eta^{sys}], \quad \dot{u}_\beta^{sys} = \frac{1}{\tau_{u_\beta}}[u_\beta - u_\beta^{sys}] \tag{20}$$

where u_η^{sys} and u_β^{sys} are the approximated actual inputs of the system. Moreover, τ_{u_η} and τ_{u_β} are the identified time response of the closed loops. To compensate the delay due to the response time of drone and on-ground winch actuators, an actuators compensation is implemented for $q \in \{r, \eta, \beta\}$:

$$u_q^d = \tau_{u_q}\dot{u}_q + u_q; \tag{21}$$

Then the system is fed by $\mathbf{u}^d = [u_r^d \quad u_\eta^d \quad u_\beta^d]^T$ to improve the system's response. The kinematic transformation block allows to transform the inputs u_{T0}^d, u_η^d and u_β^d into the desired setpoints of the drone ϕ^d, θ^d and ψ^d. This nonlinear operator is implemented by the following expressions,

$$\begin{aligned} T_D^d &= \sqrt{{u_{T0}^d}^2 + u_\eta^{d2} + u_\beta^{d2}}; \\ \phi^d &= \arcsin\left(\frac{-s_\eta s_\beta u_{T0}^d - c_\eta u_\eta^d + s_\eta s_\beta u_\beta^d}{c_\psi T_D^d}\right); \\ \theta^d &= \arctan 2\left(\frac{(c_\eta c_\beta u_{T0}^d - s_\eta u_\eta^d - c_\eta s_\beta u_\beta^d)}{c_\psi}, s_\beta u_{T0}^d + c_\beta u_\beta^d\right) \end{aligned} \tag{22}$$

E. Feedback Linearization Control

This section illustrates the 3D extension version of a 2D FL controller applied to derive a drone based fixed wing AWE system in [11] to compute $\mathbf{u} = [u_r \quad u_\eta \quad u_\beta]^T$. Firstly recall that in FL control method, the controlled system is reduced to an analogous linear system. As a result, the approach does not require any estimate and does not limit the system's operation to the linearization point's vicinity. At this stage, an intermediate linear control law is constructed to assure the asymptotic stability of the linear tracking error. The system's relative degree is 2, as can readily be seen in (18). This is the number of times the output $\mathbf{y}$ must be differentiated before the input $\mathbf{u}$ appears explicitly. Reducing (18) we get

$$\ddot{\mathbf{y}} = b(\mathbf{x}) + A(\mathbf{x})\mathbf{u} \tag{23}$$

Under the assumption that the matrix $A(\mathbf{x})$ is invertible, the control objectives is achieved with a static nonlinear control law of the form,

$$\mathbf{u} = A^{-1}(\mathbf{x})(\mathbf{v} - b(\mathbf{x})) \tag{24}$$

This nonlinear control reduces the system to a double integrator dynamics $\ddot{y} = \mathbf{v}$ such that

$$\mathbf{v} = [v_r \quad v_\eta \quad v_\beta]^T \tag{25}$$

Once the problem to solve is linear, an intermediate linear control law $\mathbf{v}$ has to be designed. In our work we implement the multivariable PID controllers for each $q \in \{r, \eta, \beta\}$, as in (26). The integral component is included to eliminate disturbances and adjust for modeling flaws, such as the unconsidered lift and drag forces.

$$v_q = \alpha_{q_{-1}} \int_0^t e_q(\tau)d\tau + \alpha_{q_0} e_q + \alpha_{q_1}\dot{e}_q + \ddot{y}_q^d \tag{26}$$

where $\mathbf{y}^d = [y_r^d \quad y_\eta^d \quad y_\beta^d]^T$ represents the desired trajectory in spherical coordinate and $e_q = (y_q^d - q)$, for $q \in \{r, \eta, \beta\}$, is the tracking error. The controllers' parameters are tuned based on Integral of the Time weighted Absolute Error (ITAE) performance index. The used characteristic polynomial for $q \in \{r, \eta, \beta\}$ is

$$P_q(s) = s^3 + 1.783w_{n_q}s^2 + 2.172w_{n_q}^2 s + w_{n_q}^3$$

where w_{n_q} is the natural frequency of the q-closed loop system. It should be noted that by selecting this option, one may obtain a stable linear tracking error with the required converging rate.
We have decided to employ an open loop control with a feedforward weight compensation for the design of u_{T0}. This open loop is represented by the following static equation $u_{T0} = T_{th}^d + m_B g sin(\beta)$, where T_{th}^d is the desired tension force in the tether. This decision was made in order to thoroughly investigate the control law on r, η and β; however, a more advanced control law may be devised for this component in order to track the tether tension faster and more precisely.

IV. Simulations Results

We have emphasised the performance of the implemented control strategy through simulations, where the drone was modeled by a very realistic model. This model doesn't only take into consideration the 6 degree of freedom dynamics but also the communication delays, motors and battery models. Fig. 2, shows the different stages which is carried out to provide the correct control actions. The Drone block represents the drone modeled as in (3)-(6) in addition to its internal control loops. While the system block corresponds to the rigid flying system. Finally, the C2S block is used to transfer the system's Cartesian coordinates to spherical ones according to (12). The Magnus Wing block, that determines the aerodynamic disturbances acting on the system, is used in simulation to study the robustness of the control strategy against wind with V_a is the apparent wind speed under a constant and homogeneous wind field of speed V_w and directed along $\vec{x}_\mathcal{G}$. The dimensions of Magnus is chosen as l_M=0.6m and r_M=0.05m. Suitable saturation to the commanded thrust force, motor-winch torque and rotational angles are included. And the desired yaw angle $\psi^d = \pi$ is assumed known constant influencing the system. Moreover, the Magnus rotational speed was set to $w_M = \frac{3}{r_M}V_w$. This leads to good aerodynamic performance of the wing.

In Table I we recapitulate the physical parameters of the system and saturation limits used in simulations. In Table II we represent the identified based simulations time constants of the drone's η-loop and β-loop. Fig. 3 represents in pink the time response of the approximated 1^{st} order model of u_β identified in (20) and in green the actual u_β of the complex simulation model. It can be seen clearly that the actual response of u_β is nonlinear. Same result was also obtained for u_η.

Fig. 4 and Fig. 5 show the system's response in 3D under different wind conditions. The system take-off at t=10s from its

TABLE I: PHYSICAL PARAMETERS

Ground Station		Drone	
Symbol	Value	Symbol	Value
m_G	0.0481 kg	m_D	0.774 kg
$\left(u^d_{r_{min}}, u^d_{r_{max}}\right)$	$\left(0,\ 8\right)$ N	$\left(T^d_{D_{min}}, T^d_{D_{max}}\right)$	$\left(3,\ 17.7\right)$ N
		$\left(\phi^d_{min}, \phi^d_{max}\right)$	$\left(-50,\ 50\right)$ deg
		$\left(\theta^d_{min}, \theta^d_{max}\right)$	$\left(-50,\ 50\right)$ deg

TABLE II: IDENTIFIED TIME RESPONSE

Ground Station		Drone	
Symbol	Value	Symbol	Value
τ_{u_r}	0.02 s	τ_{u_η}	0.115 s
		τ_{u_β}	0.121 s

initial position $[r_i \quad \eta_i \quad \beta_i]^T = [0.5 \quad 0° \quad 20°]^T$ till reaching its final position $[r_f \quad \eta_f \quad \beta_f]^T = [1.2 \quad 20° \quad 45°]^T$. Then, the system hovers at this final position for 15s. At t=25s, the system lands reaching again the initial position.

The ground motor-winch is a very fast actuator, compared to aerodynamic actuators, i.e., the drone. Moreover, as we have discussed in III-E, the ground winch is used to control the reel-out and reel-in of the tether. Thus, the r-loop natural frequency $w_{n_r} = 8$ rd/s is chosen to be bigger than that η-loop and β-loop that are controlled by the drone's actuators. Actuators compensation speeds up the closed loops, thus the natural frequencies can be increased to improve system's response without instability risk. This is impossible if the actuators dynamics are not compensated, else-wise the systems crashes. The values of the natural frequencies are represented in Table III.

TABLE III: NATURAL FREQUENCIES

	No Actuators Compensation	Actuators Compensation
w_{n_η}	3 rd/s	4 rd/s
w_{n_β}	3 rd/s	5 rd/s

In case of no wind as in Fig. 4(a), the system's response is slightly improved upon compensating the actuators. This can be clearly shown by the decreased overshoot on β in the case of actuator compensation. To study the robustness of our control strategy, we run the simulations over wind speed V_w =5m/s. Fig. 4(b) shows the importance of compensating the actuators to improve the robustness of the control strategy against wind. This is shown by comparing the β response in both cases. Compensating the actuators leads in decreasing the overshoot and the tracking error. This can be clearly obtained by comparing the system's 3D trajectories with and without actuator compensation presented in Fig. 5(a) and Fig. 5(b) respectively.

Althought the actual system can not be exactly approximated by 1^{st} order model system's response improved significantly upon adding inverse 1^{st} order actuators compensation. Moreover, the actual control value u^{sys}_β is better synchronised to the control reference u_β, as seen in Fig. 6, when implementing actuator compensation. This means that the more precise the system's

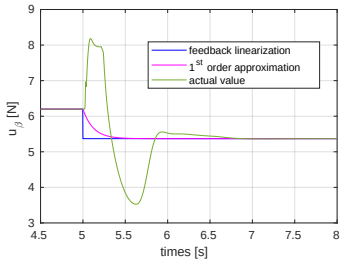

Fig. 3: Time response of u_β

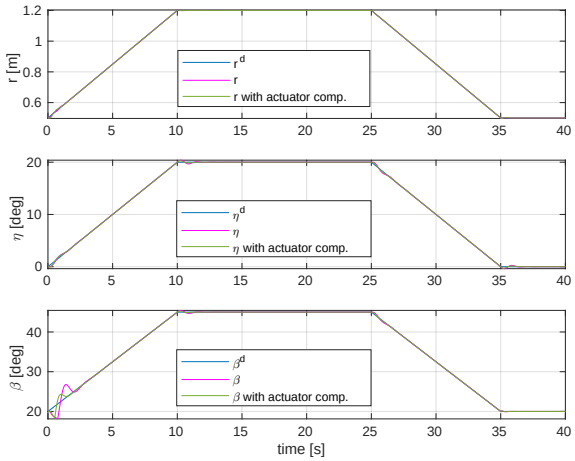

(a)

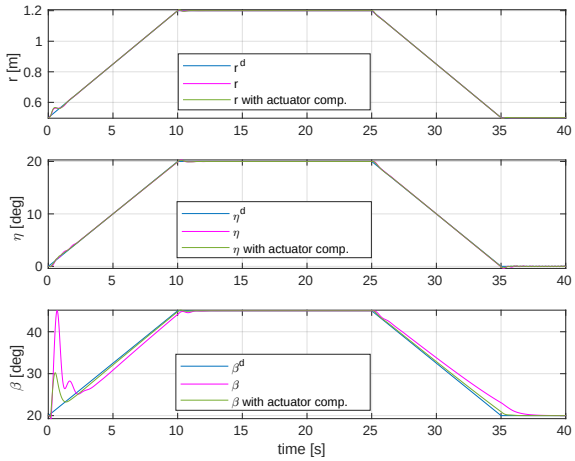

(b)

Fig. 4: Comparison of system's spherical position (a) no wind, (b) V_w= 5m/s

actuators are modeled, the more precise the system's response will be. It is important to mention that, for wind speed above $V_w = 5$ m/s, the system crashes. In this work, the aerodynamic forces acting on the system are only considered as disturbances. Increasing controller robustness against wind gusts for higher speeds may be possible by using the Magnus cylinder as actuator to benefit from aerodynamic forces to lift the system. We can see that in all case the responses of r-loop are mostly identical. This is due to the fact that the ground station motor-winch system was

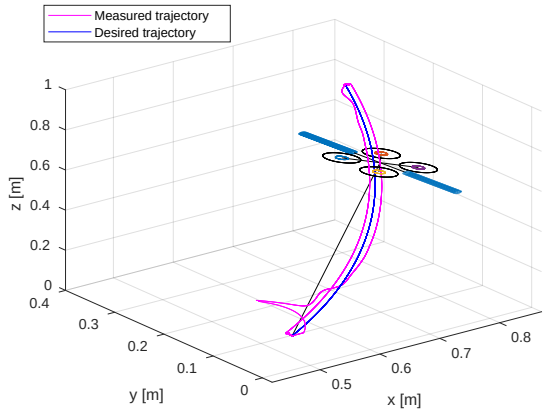

(a)

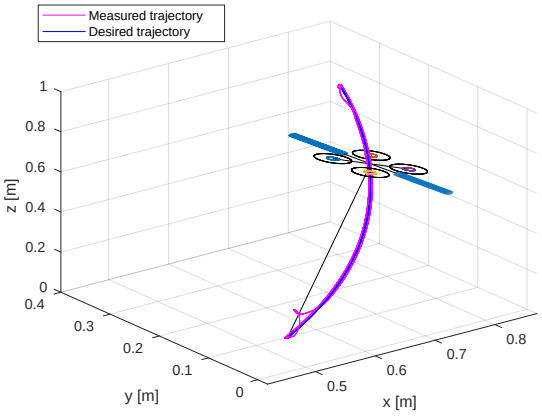

(b)

Fig. 5: System's 3D trajectory at V_w= 5m/s
(a) without actuators compensation, (b) with actuators compensation

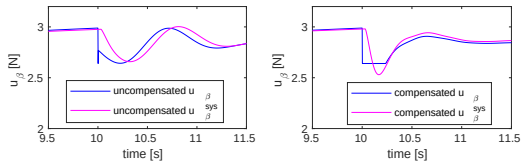

Fig. 6: Desired and actual control value u_β without and with actuator compensation

considered as very accurate with a fast dynamics, $\tau_r = 0.02s$.

V. Conclusion and Perspectives

In this paper, we have presented a control strategy based on FL control and the corresponding 3D model of drone based Magnus AWE system. The system's behavior was evaluated in complex and realistic simulation environment to support real experimental testing. It is important to mention that in this work we have neglected the effect of the reactive torque acting on the drone due to the tether force. In realistic experimentation, this additional torques could be handled by the robust built-in inner control loops of the drone. Our control strategy shows very accurate response for homogeneous and relatively low speed wind field. In the near future, we are improving our control strategy through an additional control input. These input control the Magnus's rotational speed instead of considering a constant value. This make use of aerodynamic forces to support the drone in lifting the system instead of considering them as disturbances. The absence of robustness analysis with time variable wind speed profiles, both in terms of speed and direction, is one of the key studies that is good to be considered in our future work. Moreover another proposed next step, to increase the model accuracy, is to include a more realistic tether model.

VI. Acknowledgment

The equipment used in the paper was partially funded by Equipex Robotex (ANR-10-EQPX-44-01).

References

[1] Dario Brescianini, Markus Hehn, and Raffaello D'Andrea. Nonlinear quadrocopter attitude control: Technical report. Technical report, 2013.

[2] Adel A. El-samahy and Mohamed A. Shamseldin. Brushless DC motor tracking control using self-tuning fuzzy PID control and model reference adaptive control. *Ain Shams Engineering Journal*, 9(3):341–352, September 2018.

[3] Lorenzo Fagiano, Manfred Quack, Florian Bauer, Lode Carnel, and Espen Oland. Autonomous airborne wind energy systems: accomplishments and challenges. *Annual Review of Control, Robotics, and Autonomous Systems*, 2021.

[4] Lorenzo Fagiano and Stephan Schnez. On the take-off of airborne wind energy systems based on rigid wings. *Renewable Energy*, 107, 2017.

[5] Fermi Guerrero Castellanos, Jose J. Téllez-Guzmán, Sylvain Durand, Nicolas Marchand, Jonatan Álvarez Muñoz, and V. R. Gonzalez-Diaz. Attitude stabilization of a quadrotor by means of event-triggered nonlinear control. 73(1):123–135.

[6] Yashank Gupta, Jonathan Dumon, and Ahmad Hably. Modeling and control of a magnus effect-based airborne wind energy system in crosswind maneuvers. 50(1):13878–13885, 2017. 20th IFAC World Congress.

[7] Marco M. Nicotra, Roberto Naldi, and Emanuele Garone. Nonlinear control of a tethered uav: the taut cable case. *Automatica*.

[8] Robert Mahony, Vijay Kumar, and Peter Corke. Multirotor aerial vehicles: Modeling, estimation, and control of quadrotor. *IEEE Robotics & Automation Magazine*, 19(3):20–32, 2012.

[9] Augustin Manecy. *Bio-inspired visual strategies: application to stabilization of a micro UAV and to traget tracking.* Theses, EEATS, July 2015.

[10] PX4 Organization. Px4 autopilot controller diagrams. https://docs.px4.io, Apr. 2022.

[11] Audrey Schanen, Jonathan Dumon, Nacim Meslem, Ahmad Hably, Amaury Nègre, and Alexandre Sarazin. Tethered drone-based airborne wind energy system launching and retrieving. *Journal of Guidance, Control, and Dynamics*, 44, 2021.

[12] Roland Schmehl. *Airborne wind energy: advances in technology development and research*. Springer, 2018.

[13] Davide Todeschini, Lorenzo Fagiano, Claudio Micheli, and Aldo Cattano. Control of rigid wing pumping airborne wind energy system in all operational phases. *Control Engineering Practice*, 111, 2021.

[14] Chris Vermillion, Mitchell Cobb, Fagiano Lorenzo, Rachel Leuthold, Moritz Diehl, Roy S.Smith, Tony A.Wood, Sebastian Rapp, Roland Schmehl, David Olinger, and Michael Demetriou. Electricity in the air: Insights from two decades of advanced control research and experimental flight testing of airborne wind energy systems. *Annual Review of Control*, 52, 2021.